PHOTONICS Research

Spatiotemporally reconfigurable light in degenerate laser cavities

A. Bartolo,[1,2] N. Vigne,[2] M. Marconi,[1] G. Beaudoin,[3] L. Le Gratiet,[3] K. Pantzas,[3] I. Sagnes,[3] A. Garnache,[2] and M. Giudici[1,*]

[1]Université Côte d'Azur, CNRS, Institut de Physique de Nice, 06200 Nice, France
[2]Institut d'Electronique et des Systèmes, CNRS UMR5214, 34000 Montpellier, France
[3]Centre de Nanosciences et de Nanotechnologies, CNRS UMR 9001, Université Paris-Saclay, 91120 Palaiseau, France
*Corresponding author: massimo.giudici@inphyni.cnrs.fr

Received 18 May 2023; revised 24 July 2023; accepted 24 July 2023; posted 28 July 2023 (Doc. ID 495892); published 28 September 2023

We show that a III-V semiconductor vertical external-cavity surface-emitting laser (VECSEL) can be engineered to generate light with a customizable spatiotemporal structure. Temporal control is achieved through the emission of temporal localized structures (TLSs), a particular mode-locking regime that allows individual addressing of the pulses traveling back and forth in the cavity. The spatial profile control relies on a degenerate external cavity, and it is implemented due to an absorptive mask deposited onto the gain mirror that limits the positive net gain within two circular spots in the transverse section of the VECSEL. We show that each spot emits spatially uncorrelated TLSs. Hence, the spatiotemporal structure of the light emitted can be shaped by individually addressing the pulses emitted by each spot. Because the maximum number of pulses circulating in the cavity and the number of positive net-gain spots in the VECSEL can be increased straightforwardly, this result is a proof of concept of a laser platform capable of handling light states of scalable complexity. We discuss applications to three-dimensional all-optical buffers and to multiplexing of frequency combs that share the same laser cavity.

https://doi.org/10.1364/PRJ.495892

1. INTRODUCTION

The possibility of controlling the spatiotemporal structure of light is one of the main challenges of modern photonics [1–4]. A variety of spatially complex, though stationary, light states have been demonstrated in degenerate laser cavities [5,6] by using an intracavity spatial light modulator [7,8] and metasurfaces [9,10] and through the generation of spatial localized structures (LSs) [11–14]. LSs, also called dissipative solitons, are individually addressable structures that appear in large-aspect-ratio resonators [15–18]. Because they can be used for encoding information bits, LSs have been proposed for a variety of applications to information processing [19–22]. More recently, the concept of LSs has been extended to the time domain; temporal LSs (TLSs) are addressable pulses that, exactly as their spatial counterparts, can be used as data bits for all-optical buffers and, more generally, as fundamental bricks for shaping the temporal structure of a light beam [23–28]. TLSs are also deeply related to the generation of frequency combs [29,30].

Despite significant progress, the control of the spatiotemporal structure of light is only at its beginning. Spatiotemporal mode locking states were recently reported in optical fibers [31,32], and temporally localized Turing patterns have been observed in a degenerate cavity vertical external-cavity surface-emitting laser (VECSEL) with an intracavity saturable absorber [33].

III-V semiconductor based VECSELs are promising platforms for generating spatiotemporal light states because they can gather together a large-aspect-ratio cavity and the ingredients for TLSs. While the former requires a nearly self-imaging (SI), i.e., degenerate, external cavity [34,35] and broad-area pumping, the latter is achieved in the limit of cavity round trip (τ) larger than the gain recovery time (τ_g) ($\tau > \tau_g$) and for a large modulation depth saturable absorber mirror [24,36].

In this paper, we show that a degenerate cavity VECSEL operated in the regime of TLSs can be engineered to generate light with a reconfigurable spatiotemporal structure. Spatial shaping is obtained by depositing an absorptive and non-diffractive chromium mask on top of the gain section. This mask can be drawn in an arbitrary shape, and it modulates the losses in the transverse plane of the cavity accordingly [9,37]. To provide a proof of concept of spatiotemporal control of light, we draw a positive net-gain landscape in the form of two separate round spots (hot-spots from now on). We show that each one of these spots behaves as an independent source of TLSs, and we demonstrate spatially selective addressing of individual pulses traveling into the cavity. By controlling the number

of pulses per round trip emitted by each spot, which ranges from zero (no emission) to a maximum value (N_{max}) determined by the ratio τ/τ_g, the VECSEL light emission can be customized in a large number of different spatiotemporal states.

Our realization paves the way towards an all-optical buffer where information bits can be stored in the three dimensions of the resonator. Moreover, because each hot-spot emits a frequency comb, we obtain a double frequency comb sharing the same laser medium and cavity [38–40]. Finally, we point out that the complexity of the light states generated by the described VECSEL scales with the number of hot-spots inserted and with the length of the resonator, which can both be increased straightforwardly. These developments and their impact on applications are discussed.

2. EXPERIMENTAL SETUP

The VECSEL has an L-shaped SI cavity delimited by the gain mirror (also called 1/2 VCSEL) and by a semiconductor saturable absorber mirror (SESAM), as shown in Fig. 1. VECSEL's elements are based on III-V semiconductor technology. The gain

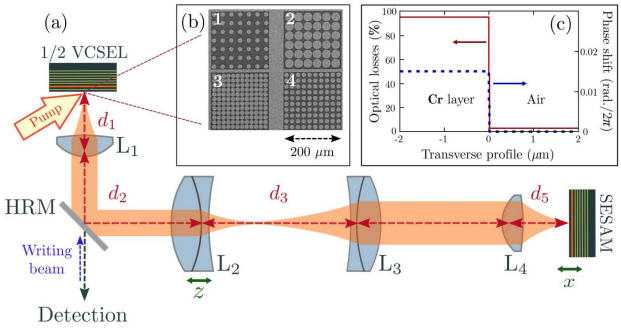

Fig. 1. (a) Experimental setup showing the L-shaped VECSEL. HRM, high reflectivity beam splitter (>99.5% at 1.060 nm). L_i are lenses whose focal lengths are $f_1 = f_4 = 8$ mm, $f_2 = 100$ mm, $f_3 = 200$ mm. While in a cold cavity, the SI condition is reached for telescopic arrangement of optical elements, the presence of a thermal lens [41] due to an optical pump beam ($f_{th} \approx \frac{10\ \text{mm W}}{P_p}$), requires slight correction to telescopic arrangement to achieve a degenerate condition. Accordingly, distances for SI condition are: $d_1 = f_1$, with d_1 the distance between gain section and L_1; $d_2 = f_1 + f_2 + z_0$, with d_2 the distance between L_1 and L_2; $d_3 = f_2 + f_3 - z_0$, with d_3 the distance between L_2 and L_3; $d_4 = f_3 + f_4$, with d_4 the distance between L_3 and L_4; and $d_5 = f_4 + x_0$, with d_5 the distance between L_4 and the SESAM. The correction terms to the telescopic configuration are given by $z_0 = -\frac{f_c^2}{2f_{th}}$ and $x_0 = -\frac{f_c^4}{2M^2 f_2^2 f_{th}}$, where $M = f_3/f_2 = 2$. For typical pump power values used in our experiment ($P_p \approx 170$ mW) and $f_{th} \approx 60$ mm: $z_0 \approx -0.53$ mm and $x_0 \approx -0.8$ μm [33]. (b) Microscope pictures of some of the masks deposited onto the gain mirror. Darker zones correspond to the Cr layer that provides losses larger than 90%. The masks shown exhibit arrangements of circular holes where the absorptive material has been removed. Diameters of holes (D) and separations between centers (T) are $D = 15$ μm, $T = 30$ μm in mask 1, $D = 30$ μm, $T = 32$ μm in mask 2, $D = 15$ μm, $T = 16$ μm in mask 3, $D = 15$ μm, $T = 20$ μm in mask 4. (c) Transverse profile of the losses and phase shift experienced by the electromagnetic field when reflected by the gain mirror around the Cr mask borderline. The Cr edge has less than 5 nm rising thickness. The phase shift of the mask is less than $2\pi/50$.

mirror is fabricated on a GaAs substrate with 12 strain-balanced InGaAs/GaAsP quantum wells (QWs) designed for barrier optical pumping and emitting at 1.06 μm. It is optically pumped at 808 nm by a flattop elliptical profile having a horizontal axis of 90 μm and a vertical one of 50 μm. The SESAM features a single strained InGaAs/GaAs QW located near the external surface leading to a recombination rate approximately two orders of magnitude faster than the gain medium. The saturated/unsaturated reflectivity modulation depth (ΔR) of the SESAM must exceed a critical value (typically $\Delta R > 8\%$ [36]) for operating the VECSEL in the TLS regime. This parameter can be varied by tuning the gain mirror and SESAM microcavity resonances (λ_G and λ_{SA}, respectively), and in the experiment here described, we fixed $\delta\lambda = \lambda_{SA} - \lambda_G = 8$ nm, leading to $\Delta R \approx 15\%$.

The degenerate external cavity is designed to be long enough to fulfill the condition for achieving the TLS regime ($\tau \approx 4.2$ ns $> \tau_g \approx 1$ ns). Moreover, the SESAM and gain mirror are placed in conjugate planes with a magnification factor $M = 2$ for increasing effectively the ratio between gain and SESAM saturation fluences. More details on VECSEL's components and on the design of the SI external cavity can be found in Ref. [33]. The VECSEL's output beam is sent to the detection part where the far-field and near-field profiles are imaged on two CCD cameras. The near field is also imaged on an array of optical fibers for spatially resolved detection at 10 GHz bandwidth (34 GHz for pulse width measurements).

A 5–10 nm thick highly absorptive (>90% at 1.06 μm) metallic (Cr) layer has been deposited on top of the gain structure. Due to e-beam lithographic post-growth process and lift-off, the shape of this layer can be arbitrarily drawn with a 5 nm spatial resolution, hence generating a non-diffractive mask that modulates the net optical gain in the transverse plane of the VECSEL [Fig. 1(c)]. A large number of masks having different shapes and pattern geometries have been drawn on the gain sample. Each mask has a size of 200 μm × 200 μm and, by shifting transversely the gain sample in front of the optical pump beam, different net-gain landscapes can be studied using the same VECSEL cavity. In this paper, we analyze the effect on the VECSEL emission of a net-gain landscape composed by circular spots (hot-spots) with sharp sub-wavelength edges, as the ones shown in Fig. 1(b). Due to the SI property of the resonator, correlation length of the emitted field is measured to be smaller than 5 μm, and cross-gain modulation between hot-spots shown in Fig. 1(b) is negligible. It is worth noting that the presence of these masks increases dramatically the total amount of losses in the VECSEL cavity, and lasing emission could be obtained only in presence of hot-spots having a diameter larger than 15 μm. Finally, we have used mask 2 in Fig. 1(b) whose hot-spots have a diameter of 30 μm, thus enabling output intensities strong enough to be detected by fast detectors. This mask features the highest density of hot-spots (32 μm distance between their centers), and, accordingly, two hot-spots fit in the pumped area.

3. EXPERIMENTAL RESULTS

The VECSEL spatiotemporal emission is described in Fig. 2. The near-field and far-field time averaged profiles reveal that each hot-spot emits a couple of tilted beams whose transverse

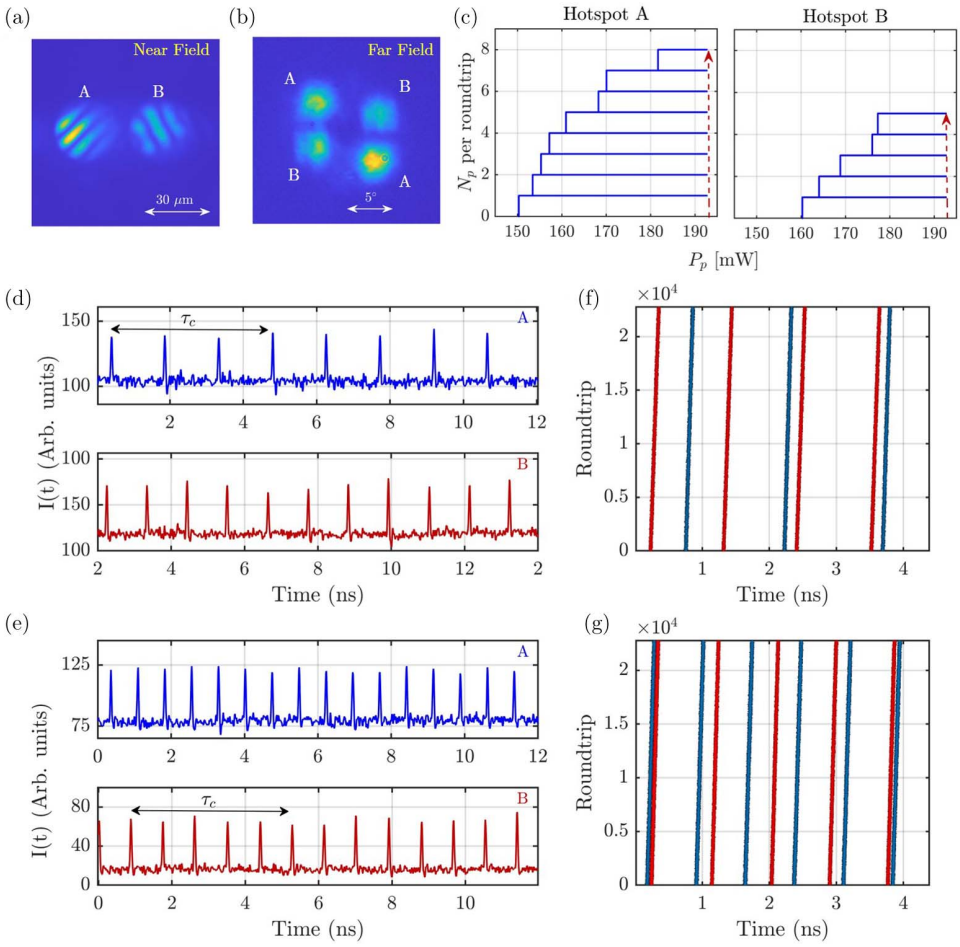

Fig. 2. Spatiotemporal behavior of the light emitted by the VECSEL with two hot-spots in the gain section (A and B). (a), (b) Time-averaged near-field and far-field profiles of the VECSEL emission. (c) Bifurcation diagrams of the mode-locking emission from each hot-spot. These diagrams are obtained according to the following procedure: pump power P_p is increased from zero up to the VECSEL threshold value ($P_{p,\mathrm{th}} = 192.5$ mA), where an off solution becomes unstable at the advantage of mode-locked emission having $N_{\max}$ pulses per round trip. Then, P_p is decreased until the emission jumps to the emission having $N_{\max} - 1$ pulses per round trip. At this point, the stability of this solution is tested by increasing again P_p up to $P_{p,\mathrm{th}}$ and by decreasing it down to the point where the emission jumps to the solution with $N_{\max} - 2$ pulses per round trip. This is repeated for every solution with a number of pulses per round trip different from zero, until the system jumps to the off solution. The difference in the number $N_{\max}$ of pulses per round trip for the two hot-spots is due to a non-perfectly homogeneous level of pumping of the two regions. (d), (e) Two different emission states obtained for the same parameter values in the multi-stable region ($P_p = 185$ mW). The blue (red) time trace represents the intensity emitted by hot-spot A (B). In panel (d), we show the state ($N_A = 3, N_B = 4$), while in panel (e), we show the state ($N_A = 6, N_B = 5$). Space–time diagrams of these states, picturing the evolution of pulses emitted round trip after round trip, are represented in panels (f) ($N_A = 3, N_B = 4$) and (g) ($N_A = 6, N_B = 5$).

wave vectors have the same modulus and opposite direction ($\pm\vec{k}_t$). The interference of the two beams generates a stripe pattern in the near-field profile at each spot. Tilted beam emission is typical of degenerate cavities [42–45], and it is related to spherical aberrations of the optical elements of the cavity, which become more and more relevant close to SI conditions. Moreover, the interference pattern in the near field enables an effective saturation of the SESAM. It is worth noting that the direction of the transverse wave vectors can be different for each spot. In the situation shown in Fig. 2, the two hot-spots emit beams that are in orthogonal directions, thus allowing separation of the two emissions in both near and far fields. Slight tilting of the optical elements enables some control in these directions. The direction of the tilted beams emitted by a hot-spot can be imposed by introducing some ellipticity in the hot-spot shape, thus breaking the azimuthal symmetry and forcing a well determined direction $\pm\vec{k}_t$.

The analysis of the VECSEL emission in the time domain reveals that each spot emits mode-locked solutions with a number of pulses per round trip (N_A and N_B), which can be varied by changing the pump value, as shown in Fig. 2(c). These stability diagrams reveal that each hot-spot features multi-stability between different mode-locked states with the number of pulses per round trip ranging from $N_A = 0$ (no emission) to $N_{A,\max} = 8$ and from $N_B = 0$ (no emission) to $N_{B,\max} = 5$. This multi-stability is a signature of TLSs that, in our VECSELs, are emitted by two spatially independent hot-spots. In the multi-stable range, $160\ \mathrm{mW} < P_p < 190\ \mathrm{mW}$,

different combinations of N_A and N_B can be obtained in the VECSEL emission simply by perturbing the system. This can be done by opening and closing the light path inside the cavity. Two examples of these combinations are given in Figs. 2(d) and 2(f) where $N_A = 3$, $N_B = 4$ and in Figs. 2(e) and 2(g) where $N_A = 6$, $N_B = 5$. The duration of the pulses cannot be resolved by our detection bandwidth; hence the pulse width is smaller than 20 ps. Time-averaged output power from each spot is about 20 μW.

These experimental evidences show that a degenerate cavity can host two spatially decorrelated sources of TLSs emitting beams with different transverse wave vectors, thus providing spatiotemporally structured light. In addition, because TLSs are individually addressable pulses, we can control the number of pulses emitted by each spot by perturbing locally the pump intensity. This control is achieved by injecting a short pump pulse having a waist of only 7 μm, thus targeting a single hot-spot. The system is prepared in the multi-stable parameter region, and the amplitude of the addressing pump pulse is chosen to bring the system beyond the upper limit of the multi-stable region ($P_p > 190$ mW). This perturbation is applied synchronously with the cavity round trip for about 1000 round trips. In Fig. 3(a), we demonstrate the addressing of a pulse emitted by hot-spot A starting from the initial condition where $N_A = 0$, $N_B = 3$. This process is illustrated by using a space–time diagram where the writing pump pulse is represented with a color scale, while the trajectory of each emitted pulse is represented by a black trace. The writing pulse is applied at round trip #10,000 and it is sufficiently short to switch on a single TLS. The written pulse persists after the perturbation is removed. It is worth noting that no effect is produced onto the emission from hot-spot B during and after the writing process. In Fig. 3(b), we repeat the operation by targeting hot-spot B starting from the initial condition $N_A = 2$ and $N_B = 0$. Other initial conditions can be chosen with similar results, provided that the addressing pulse is separated in time from the preexisting TLS of at least τ_g. Pulse erasure is also obtained by perturbing a single hot-spot with a negative pump pulse, as done in Ref. [33].

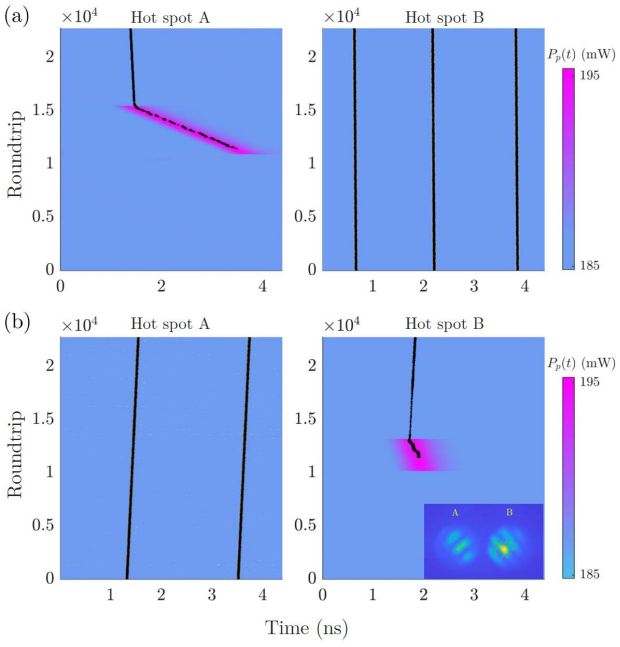

Fig. 3. Space–time diagram of the writing process of TLS in each hot-spot. (a) Writing of one LS in hot-spot A while hot-spot B is emitting three TLSs per round trip ($N_B = 3$). The writing pump pulse is applied at round trip #10,000, and spot A emits a TLS that follows the timing of the perturbation pulse that is incidentally different from the round trip of the system. When the writing pulse is removed at round trip #15,000, the solution $N_A = 1$ remains stable. (b) Writing of one TLS in the hot-spot B while hot-spot A is emitting $N_A = 2$ TLSs per round trip. In the inset, we show the time-averaged near-field emission of the VECSEL during application of the perturbation to hot-spot B. The waist of the perturbation beam can be compared with the interference fringes.

4. DISCUSSION

This result provides a demonstration of a laser source capable of generating spatiotemporally structured light beams organized on two spatial channels and on a number of pulses in each channel ranging from zero to eight in hot-spot A, and from zero to five in hot-spot B. If we identify light states simply by the number of pulses emitted by each hot-spot (N_A, N_B), the number of different light states that can be obtained is 54. In general, if we consider that the value of $N_{\max}$ is the same for all hot-spots, the number of combinations in a VECSEL with n hot-spots is given by $(N_{\max} + 1)^n$. The maximum number of TLSs per channel ($N_{\max}$) depends on the ratio between cavity round trip and gain recovery time (τ/τ_g) [24], which can be increased straightforwardly by using longer resonators. On the other hand, there are no technological obstacles to increase n up to eight by doubling the optical pump size. For larger sizes, the total pump power will exceed 1 W, and thermal management solutions of the gain section will be necessary. These solutions require additional technological steps in the realization of the gain mirror as, for example, integration of a diamond heat spreader. These considerations reveal that the demonstrated laser platform is capable of handling light states of scalable complexity.

The generated light states are particularly suitable for applications to information processing, since each pulse circulating in the cavity can be used to encode an information bit. Accordingly, the VECSEL described in this paper can be used as an all-optical buffer whose memory size is given by the product $n \cdot N_{\max}$. Another possible application is related to the use of each hot-spot as a source of a frequency comb. Accordingly, the VECSEL described enables multiplexing of frequency combs sharing the same active/passive medium, i.e., the same noise sources, thus increasing the mutual coherence required for multi-frequency comb operations [38–40]. Moreover, the possibility of varying the comb tooth spacing of each hot-spot by addressing the number of pulses per round trip emitted, provides an additional degree of freedom for controlling the spectral line density of the resulting RF comb.

The evolution of the TLSs round trip after round trip, shown in Figs. 2(f) and 2(g), reveals that the periodicity of the TLSs is the same for both hot-spots regardless of the number of pulses emitted per round trip, in contrast to previous observations in TLS emitters with homogeneous net-gain

profiles [26]. Then, a form of synchronization between the two hot-spots takes place in our VECSEL due to the fact that they share the same active and passive media. This period locking has been observed for different combinations of N_A and N_B, and it persists in emission states where the difference between N_A and N_B is maximized ($|N_A - N_B| = 4$).

This phenomenon is beneficial for data buffering since a common clock can be established for all channels of the buffer. On the other hand, for multi-frequency comb generation, it is required that the pulse trains emitted by the two hot-spots have incommensurate repetition rates. This can be obtained by controlling locally the continuous wave (CW) pump power impinging each hot-spot. To this aim, we superpose to the homogeneous pump two pump beams having a waist of 7 μm and whose power, P_A and P_B, can be controlled independently. Due to the multi-stable response of the VECSEL, an arbitrary emission state (N_A, N_B) is robust upon variation of P_A and P_B in the interval where states N_A and N_B are stable [see Fig. 2(c)]. Because the repetition rate of the emitted TLSs depends on the pumping level, the local pump power P_A (P_B) enables to tune slightly the period τ_A (τ_B) of the TLSs emitted by hot-spot A (B) [26]. In Fig. 4, we have set the emission state $N_A = 1$, $N_B = 3$ and induced a difference between τ_A and τ_B by increasing P_A over P_B. This difference is evident in the space–time diagram of Fig. 4, showing the walk-off of the pulses emitted by hot-spot B versus the pulse emitted by hot-spot A. This walk-off is approximately 1 ns after 22,500 round trips, thus leading to $|\tau_A - \tau_B| = 4.4 \times 10^{-5}$ ns. Accordingly, the combination of frequency combs generated by hot-spots A and B leads to an RF spectrum having lines separated by $\Delta f_r = |1/\tau_A - 1/\tau_B| = 2.5$ kHz. The full characterization of this double frequency comb is out of the scope of this paper and will be presented elsewhere.

In conclusion, we have shown that degenerate III-V semiconductor VECSELs with an intracavity saturable absorber are a promising platform for generating light with an addressable spatiotemporal structure. Control of the spatial profile relies on the introduction of two spots of positive net-gain onto the gain section, while temporal control of light is obtained due to the properties of TLSs. By controlling the number of pulses emitted by each spot, the light emitted can be reconfigured in a large variety of different spatiotemporal states. Because each pulse can be used to encode an information bit, the VECSEL described materializes an all-optical three-dimensional buffer. Moreover, we have shown that each spot can be used as a frequency comb source, thus leading to a double frequency comb in the same laser cavity. These proofs of concept are based on two spatial channels and a small number of pulses per round trip; however, these figures can be increased straightforwardly by increasing the size of the pump and length of the cavity.

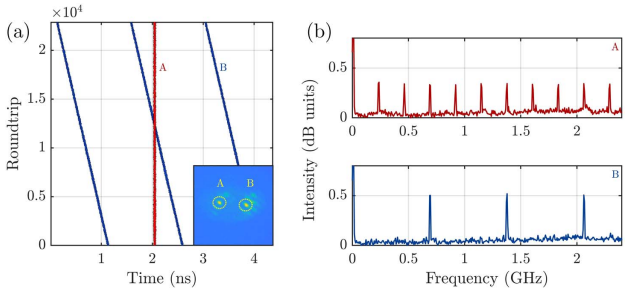

Fig. 4. (a) Evolution of the TLS emitted by hot-spots A (red trace) and B (blue trace) in presence of two continuous wave (CW) 7-μm-waist pump beams targeting hot-spots A and B. Their powers P_A and P_B can be controlled independently. Here $P_A = 35$ mW and $P_B = 45$ mW. Both narrow waist pump beams are superimposed to the homogeneous pump beam, which is kept to a power $P_p = 120$ mW. Inset: near-field time-averaged emission of the VECSEL showing the presence of the two 7-μm-waist independent pumps targeting hot-spots A and B. (b) Power spectra of the two outputs from hot-spots A (red trace) and B (blue trace).

Funding. Région PACA (OPTIMAL); Agence Nationale de la Recherche (ANR-18-CE24-0002).

Acknowledgment. This work was supported by the French RENATECH network. The INPHYNI Group acknowledges ANR and Région PACA.

Disclosures. The authors declare no conflicts of interest.

Data Availability. Data underlying the results presented in this paper are not publicly available at this time but may be obtained from the authors upon reasonable request.

REFERENCES

1. A. Forbes, M. de Oliveira, and M. Dennis, "Structured light," Nat. Photonics **15**, 253–262 (2021).
2. M. Piccardo, V. Ginis, A. Forbes, S. Mahler, A. A. Friesem, N. Davidson, H. Ren, A. H. Dorrah, F. Capasso, F. T. Dullo, B. S. Ahluwalia, A. Ambrosio, S. Gigan, N. Treps, M. Hiekkamäki, R. Fickler, M. Kues, D. Moss, R. Morandotti, J. Riemensberger, T. J. Kippenberg, J. Faist, G. Scalari, N. Picqué, T. W. Hänsch, G. Cerullo, C. Manzoni, L. A. Lugiato, M. Brambilla, L. Columbo, A. Gatti, F. Prati, A. Shiri, A. F. Abouraddy, A. Alù, E. Galiffi, J. B. Pendry, and P. A. Huidobro, "Roadmap on multimode light shaping," J. Opt. **24**, 013001 (2022).
3. L. G. Wright, W. H. Renninger, D. N. Christodoulides, and F. W. Wise, "Nonlinear multimode photonics: nonlinear optics with many degrees of freedom," Optica **9**, 824–841 (2022).
4. N. Davidson, S. Mahler, A. Friesem, and A. Forbes, "Complex-light lasers," Opt. Photon. News **33**, 26–33 (2022).
5. H. Cao, R. Chriki, S. Bittner, A. A. Friesem, and N. Davidson, "Complex lasers with controllable coherence," Nat. Rev. Phys. **1**, 156–168 (2019).
6. S. Knitter, C. Liu, B. Redding, M. K. Khokha, M. A. Choma, and H. Cao, "Coherence switching of a degenerate vecsel for multimodality imaging," Optica **3**, 403–406 (2016).
7. C. Tradonsky, S. Mahler, G. Cai, V. Pal, R. Chriki, A. A. Friesem, and N. Davidson, "High-resolution digital spatial control of a highly multimode laser," Optica **8**, 880–884 (2021).
8. S. Ngcobo, I. Itvine, L. Burger, and A. Forbes, "A digital laser for on-demand laser modes," Nat. Commun. **4**, 2289 (2013).
9. M. S. Seghilani, M. Myara, M. Sellahi, L. Legratiet, I. Sagnes, G. Beaudoin, P. Lalanne, and A. Garnache, "Vortex laser based on III-V semiconductor metasurface: direct generation of coherent Laguerre-Gauss modes carrying controlled orbital angular momentum," Sci. Rep. **6**, 38156 (2016).
10. M. Piccardo, M. de Oliveira, A. Toma, V. Aglieri, A. Forbes, and A. Ambrosio, "Vortex laser arrays with topological charge control and self-healing of defects," Nat. Photonics **16**, 359–365 (2022).

11. S. Barland, J. R. Tredicce, M. Brambilla, L. A. Lugiato, S. Balle, M. Giudici, T. Maggipinto, L. Spinelli, G. Tissoni, T. Knödl, M. Miller, and R. Jäger, "Cavity solitons as pixels in semiconductor microcavities," Nature **419**, 699–702 (2002).
12. Y. Tanguy, T. Ackemann, W. J. Firth, and R. Jäger, "Realization of a semiconductor-based cavity soliton laser," Phys. Rev. Lett. **100**, 013907 (2008).
13. P. Genevet, S. Barland, M. Giudici, and J. R. Tredicce, "Cavity soliton laser based on mutually coupled semiconductor microresonators," Phys. Rev. Lett. **101**, 123905 (2008).
14. P. Genevet, S. Barland, M. Giudici, and J. R. Tredicce, "Bistable and addressable localized vortices in semiconductor lasers," Phys. Rev. Lett. **104**, 223902 (2010).
15. N. N. Rosanov and G. V. Khodova, "Diffractive autosolitons in nonlinear interferometers," J. Opt. Soc. Am. B **7**, 1057–1065 (1990).
16. L. Lugiato, "Introduction to the feature section on cavity solitons: an overview," IEEE J. Quantum Electron. **39**, 193–196 (2003).
17. P. Mandel and M. Tlidi, "Transverse dynamics in cavity nonlinear optics (2000–2003)," J. Opt. B Quantum Semiclass. Opt. **6**, R60 (2004).
18. T. Ackemann, W. J. Firth, and G. Oppo, "Chapter 6: Fundamentals and applications of spatial dissipative solitons in photonic devices," in *Advances in Atomic Molecular and Optical Physics*, P. R. B. E. Arimondo and C. C. Lin, eds., Vol. **57** of Advances in Atomic Molecular and Optical Physics (Academic, 2009), pp. 323–421.
19. P. Coullet, C. Riera, and C. Tresser, "A new approach to data storage using localized structures," Chaos **14**, 193–198 (2004).
20. F. Pedaci, P. Genevet, S. Barland, M. Giudici, and J. R. Tredicce, "Positioning cavity solitons with a phase mask," Appl. Phys. Lett. **89**, 221111 (2006).
21. F. Pedaci, G. Tissoni, S. Barland, M. Giudici, and J. R. Tredicce, "Mapping local defects of extended media using localized structures," Appl. Phys. Lett. **93**, 111104 (2008).
22. F. Pedaci, S. Barland, E. Caboche, P. Genevet, M. Giudici, J. R. Tredicce, T. Ackemann, A. J. Scroggie, W. J. Firth, G.-L. Oppo, G. Tissoni, and R. Jäger, "All-optical delay line using semiconductor cavity solitons," Appl. Phys. Lett. **92**, 011101 (2008).
23. F. Leo, S. Coen, P. Kockaert, S. Gorza, P. Emplit, and M. Haelterman, "Temporal cavity solitons in one-dimensional Kerr media as bits in an all-optical buffer," Nat. Photonics **4**, 471–476 (2010).
24. M. Marconi, J. Javaloyes, S. Balle, and M. Giudici, "How lasing localized structures evolve out of passive mode locking," Phys. Rev. Lett. **112**, 223901 (2014).
25. M. Marconi, J. Javaloyes, S. Barland, S. Balle, and M. Giudici, "Vectorial dissipative solitons in vertical-cavity surface-emitting lasers with delays," Nat. Photonics **9**, 450–455 (2015).
26. P. Camelin, J. Javaloyes, M. Marconi, and M. Giudici, "Electrical addressing and temporal tweezing of localized pulses in passively-mode-locked semiconductor lasers," Phys. Rev. A **94**, 063854 (2016).
27. S. Barland, S. Coen, M. Erkintalo, M. Giudici, J. Javaloyes, and S. Murdoch, "Temporal localized structures in optical resonators," Adv. Phys. X **2**, 496–517 (2017).
28. N. Englebert, C. Mas-Arabi, P. Parra-Rivas, S. Gorza, and F. Leo, "Temporal solitons in a coherently driven active resonator," Nat. Photonics **15**, 536–541 (2021).
29. T. Herr, V. Brasch, J. D. Jost, C. Y. Wang, N. M. Kondratiev, M. L. Gorodetsky, and T. J. Kippenberg, "Temporal solitons in optical microresonators," Nat. Photonics **8**, 145–152 (2014).
30. A. Bao, H. Cooper, M. Rowley, L. Di Lauro, J. S. Totero Gongora, S. T. Chu, B. E. Little, G.-L. Oppo, R. Morandotti, D. J. Moss, B. Wetzel, M. Peccianti, and A. Pasquazi, "Observation of mode-locked spatial laser solitons," Nat. Photonics **13**, 384–389 (2019).
31. L. G. Wright, D. N. Christodoulides, and F. W. Wise, "Spatiotemporal mode-locking in multimode fiber lasers," Science **358**, 94–97 (2017).
32. L. G. Wright, P. Sidorenko, H. Pourbeyram, Z. M. Ziegler, A. Isichenko, B. A. Malomed, C. R. Menyuk, D. N. Christodoulides, and F. W. Wise, "Mechanisms of spatiotemporal mode-locking," Nat. Phys. **16**, 565–570 (2020).
33. A. Bartolo, N. Vigne, M. Marconi, G. Beaudoin, K. Pantzas, I. Sagnes, G. Huyet, F. Maucher, S. V. Gurevich, J. Javaloyes, A. Garnache, and M. Giudici, "Temporal localized Turing patterns in mode-locked semiconductor lasers," Optica **9**, 1386–1393 (2022).
34. A. E. Siegman, *Lasers* (University Science Books, 1986).
35. J. A. Arnaud, "Degenerate optical cavities," Appl. Opt. **8**, 189–196 (1969).
36. P. Camelin, C. Schelte, A. Verschelde, A. Garnache, G. Beaudoin, I. Sagnes, G. Huyet, J. Javaloyes, S. Gurevich, and M. Giudici, "Temporal localized structures in mode-locked vertical external-cavity surface-emitting laser," Opt. Lett. **43**, 5367–5370 (2018).
37. S. Blin, R. Paquet, M. Myara, B. Chomet, L. Le Gratiet, M. Sellahi, G. Beaudoin, I. Sagnes, G. Ducournau, P. Latzel, J.-F. Lampin, and A. Garnache, "Coherent and tunable THz emission driven by an integrated III–V semiconductor laser," IEEE J. Sel. Top. Quantum Electron. **23**, 1500511 (2017).
38. I. Coddington, N. Newbury, and W. Swann, "Dual-comb spectroscopy," Optica **3**, 414–426 (2016).
39. S. M. Link, A. Klenner, M. Mangold, C. A. Zaugg, M. Golling, B. W. Tilma, and U. Keller, "Dual-comb modelocked laser," Opt. Express **23**, 5521–5531 (2015).
40. J. Pupeikis, B. Willenberg, S. L. Camenzind, A. Benayad, P. Camy, C. R. Phillips, and U. Keller, "Spatially multiplexed single-cavity dual-comb laser," Optica **9**, 713–716 (2022).
41. A. Laurain, M. Myara, G. Beaudoin, I. Sagnes, and A. Garnache, "High power single–frequency continuously–tunable compact extended–cavity semiconductor laser," Opt. Express **17**, 9503–9508 (2009).
42. X. Hachair, S. Barbay, T. Elsass, I. Sagnes, and R. Kuszelewicz, "Transverse spatial structure of a high Fresnel number vertical external cavity surface emitting laser," Opt. Express **16**, 9519–9527 (2008).
43. A. A. Bartolo González, "Spatial organization of localized pulses in a self-imaging vertical external cavity surface emitting laser," Ph.D. Thesis (Université Côte d'Azur, 2022).
44. N. Vigne, "3D structured coherent light state emitted by a self imaging laser cavity based on semiconductor VECSEL technology," Ph.D. Thesis (Université de Montpellier, 2022).
45. S. Gurevich, F. Maucher, N. Vigne, A. A. Bartolo, M. Marconi, G. Beaudoin, K. Pantzas, I. Sagnes, A. Garnache, M. Giudici, and J. Javaloyes, "Quartic beams of temporal solitons in a nearly-degenerated laser cavity," arXiv, arXiv:2306.11359 (2023).